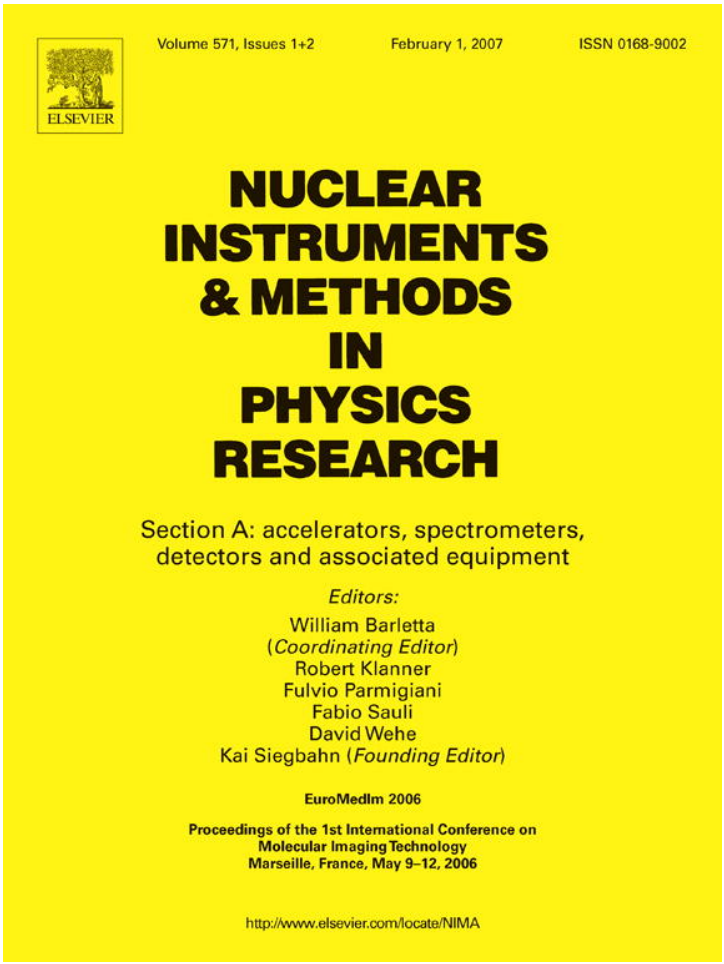

Available online at www.sciencedirect.com
ScienceDirect
Nuclear Instruments and Methods in Physics Research A 571 (2007) 134–141
NUCLEAR INSTRUMENTS & METHODS IN PHYSICS RESEARCH Section A
www.elsevier.com/locate/nima

Recent results with a segmented Hybrid Photon Detector for a novel, parallax-free PET Scanner for Brain Imaging

A. Braem[a], E. Chesi[a], C. Joram[a], S. Mathot[a], J. Séguinot[a], P. Weilhammer[a,*], F. Ciocia[b], R. De Leo[b], E. Nappi[b], I. Vilardi[b], A. Argentieri[c], F. Corsi[c], A. Dragone[c], D. Pasqua[c]

[a]*CERN, PH Department, CH-1211 Geneva, Switzerland*
[b]*INFN, Sezione di Bari and University of Bari, Bari, Italy*
[c]*INFN, Sezione di Bari and Politechnic of Bari, Bari, Italy*

Available online 7 November 2006

Abstract

We describe the design, fabrication and test results of a segmented Hybrid Photon Detector with integrated auto-triggering front-end electronics. Both the photodetector and its VLSI readout electronics are custom designed and have been tailored to the requirements of a recently proposed novel geometrical concept of a Positron Emission Tomograph. Emphasis is laid on the PET specific features of the device. The detector has been fabricated in the photocathode facility at CERN.

PACS: 87.58.Fg; 85.60.Ha; 85.40.−e

Keywords: Positron Emission Tomography; PET; HPD; Front-end electronics

1. Introduction

Hybrid Photon Detectors (HPDs) are advanced photodetectors whose features and properties provide new opportunities for medical imaging. The development and some recent results from a segmented HPD discussed in this article is part of an R&D program focused on a novel geometrical concept of a Positron Emission Tomography (PET). It allows for a parallax-free 3D reconstruction of the positron source distribution with high spatial and energy resolution over the complete Field of View (FOV).

The 3D axial concept was proposed[1] as a competitive and innovative approach, mainly for a high-resolution brain PET scanner. Sensitivity enhancement is achieved by identifying a fraction of events that underwent Compton scattering in the segmented scintillation detector, leading to high-quality image reconstruction and reduced scanning time.

The PET concept (see Refs. [1–3]) is based on camera modules consisting of axially oriented matrices of 16×13 long polished LYSO[2] scintillator bars (e.g. $3.2 \times 3.2 \times 150\,\mathrm{mm}^3$) optically coupled at both ends to two PET-HPDs (see Fig. 1). The auto-triggering front-end electronics (FEE) is encapsulated in the detector body. A number of camera modules form a complete cylinder around the patient.

The scintillation light produced by a γ interacting in a polished crystal bar propagates by total internal reflection to the ends with an absorption characterized by the bulk attenuation length λ of the crystal and the light path length. The transverse coordinates x and y of the interaction point are derived from the address of the hit crystal. In the first approximation and in the absence of cross-talk, the resolution is $\sigma_{x,y} = 3.2\,\mathrm{mm}/\sqrt{12} \approx 0.9\,\mathrm{mm}$. The x–y measurement defines accurately the depth of interaction (DOI) and consequently suppresses the parallax error when reconstructing the Line of Response (LOR) of a "True"

*Corresponding author.
E-mail address: Peter.Weilhammer@cern.ch (P. Weilhammer).

[1]Patent application filed under PCT/EP02/07967, international publication number WO 2004/008177 A1.

[2]The LYSO ($LuYSiO_5$:Ce) scintillation crystal has the following main properties: Photon yield: 32 ph/keV, decay time: 48 ns, peak wavelength: 420 nm, photo fraction at 511 keV: 34.4%.

0168-9002/$ - see front matter © 2006 Elsevier B.V. All rights reserved.
doi:10.1016/j.nima.2006.10.047

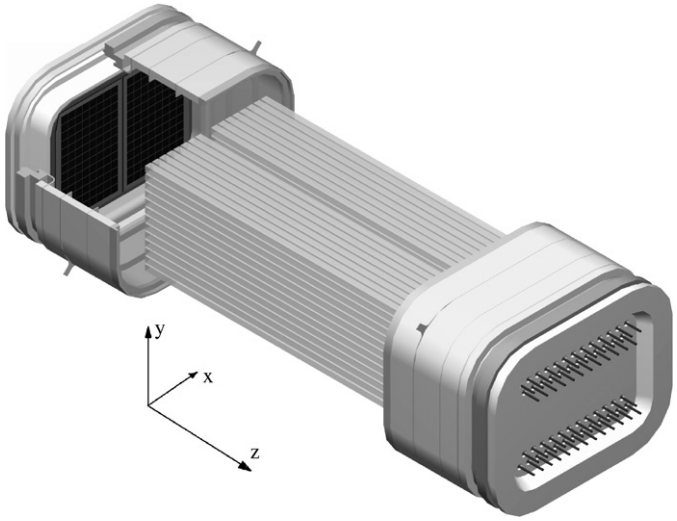

Fig. 1. Drawing of a camera module consisting of a matrix of 150 mm long scintillator crystals read out by two (rectangular) HPDs.

event with two identified back to back 511 keV γ's emitted in the positron annihilation process. The third (axial) coordinate z, is derived classically from the ratio of the photoelectron yields N_1, N_2, measured at the two ends of the crystal bar,

$$z = \tfrac{1}{2}(\lambda \ln(N_1/N_2) + L), \quad (L \text{ is the bar length})$$

with an accuracy which depends on the light absorption length λ relative to the length of the bar [1,4]. Moreover, the energy loss in a crystal bar, either by photoelectric effect or by Compton scattering, is determined after correction for the light absorption and calibration from the relation,

$$N_0 = N_1 e^{z/\lambda} + N_2 e^{(L-z)/\lambda}.$$

A precise measurement of the energy loss in the matrix is important to determine the γ energy in order to reject scatter events in the organic tissues and, for the discussed concept, to identify the first interaction point in the crystal matrix when a Compton interaction occurs in to the forward hemisphere.

A 511 keV γ, which looses its energy by photoelectric effect in a polished LYSO crystal bar, generates photoelectron yields N_1, N_2 of about 500 in each of the HPDs for a standard bi-alkali photocathode response. Assuming a maximum photo detector gain of 5×10^3 (see Section 3.3), the corresponding charge at the input of the pre-amplifier corresponds to about 400 fC. In order to safely detect a 50 keV recoil electron from Compton interactions, the electronic detection threshold must be $\leqslant 30$ fC. Such a low threshold causes a large increase of the counting rate per electronic channel, which would result in a high accidental coincidence rate. To solve the problem, the HPD and the readout electronic are designed to select two coincident γ's for only those events for which the total energy lost in the full scintillator matrix is found within an energy window centred around 511 keV. This is obtained by measuring the induced charge signal on the back plane of the Si sensor (see below), which provides a signal proportional to the total light-yield emitted in the matrix.

2. The hybrid photon detector: PET-HPD

HPDs have been chosen for the PET project because of their unique properties for medical imaging applications compared to the commercially available standard photon detectors (Multi-Anode PMT, Avalanche Photodiodes, etc.). They combine an exceptional spatial and energy resolution with a great flexibility of design (size, geometry). Moreover, HPDs of large sensitive area and granularity can easily be tailored as required for the readout of a scintillator matrix.

The charge gain of HPDs is achieved in a single-stage dissipation process. The linearity of the response with the incident light is excellent over a large dynamic range and is usually only limited by the performance of the electronics. Moreover, the gain is unaffected by variations of the detector temperature.

For photoelectrons (pe's) accelerated up to energies E of typically 15–20 keV, the dispersion of the gain (the gain being defined by the number of e–h pairs created per pe in the depleted volume of the Si sensor) is affected by the fluctuation of the energy loss ΔE (straggling) in the inactive entrance layer of the Si sensor,[3] and by those (~18%) pe's that are scattered back from the sensor and deposit only partially their kinetic energy. This last effect is almost independent of the acceleration potential.

The charge gain of the HPD is $g = (E - \Delta E)/w$ with $w = 3.62$ eV per created electron–hole pair and its spread $\sigma_g = [\sigma^2(E/w) + \sigma^2(\Delta E/w)]^{1/2}$, with $\sigma(E/w) = (FgN)^{1/2}$, where F is the Fano factor ($F = 0.14$ in Si) and N the number of pe's. The straggling $\sigma(\Delta E/w)$ depends on the acceleration voltage, because of the finite thickness of the inactive entrance layer consisting of a conductive Al layer deposited on the sensor surface for the polarization of the sensor and an ohmic n^+ implant. At high acceleration potential, as will be shown below, the straggling becomes negligible. Experimentally, ignoring the straggling effect at high energies, the measured charge distribution can be characterized by a Gaussian with mean value $\mu = gN$ and variance $\sigma = g(\mathrm{ENF}{*}N)^{1/2}$, where ENF is the so-called excess noise factor (ENF = 1.045 for HPD[4]). Consequently, the number of pe's is simply determined by $N = ENF{*}(\mu/\sigma)^2$.

An important advantage of HPDs for the axial PET concept is, as discussed above, the possibility of reading out the induced signal on the Si sensor back plane,

[3]The Si sensor is mounted upside down, such that the photoelectrons hit the nonsegmented backside.

[4]The ENF of a HPD is essentially due to the back scattering phenomenon mentioned in Section 2. The value ENF = 1.045 follows both from an analytical and M.C. calculation.

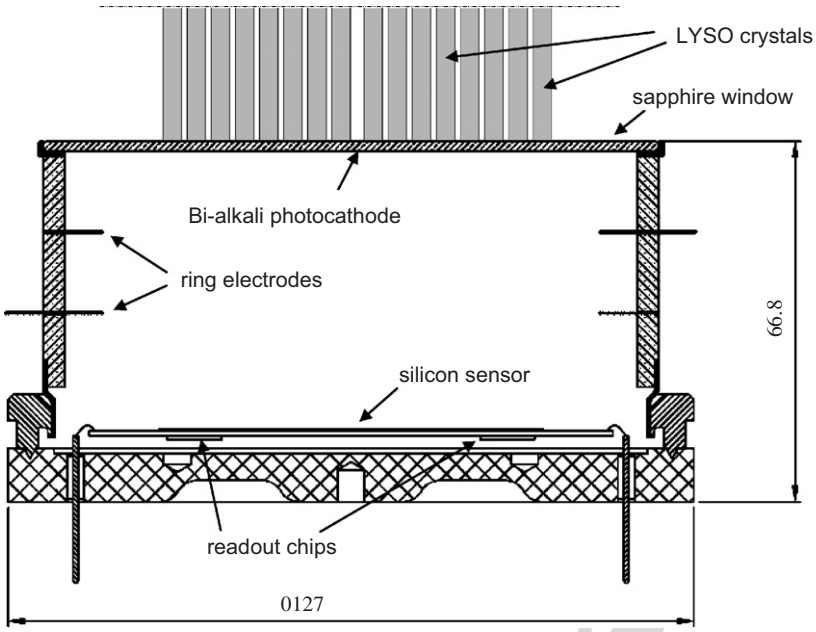

Fig. 2. Cross-section of the round PET-HPD prototype with scintillator crystals coupled to it.

providing a fast measurement of the total charge deposited in the depleted Si bulk. This unique feature allows for a simple and fast photon energy discrimination. Moreover the back plane's fast signals can be used to detect "True" events in coincident detector modules with a time resolution below 10 ns [1].

2.1. The prototype PET-HPD

The prototype PET-HPD developed at CERN [5] is a round[5] proximity-focused HPD with a bi-alkali photocathode (QE of about 25% at peak wavelength) deposited on a thin (1.8 mm) flat sapphire entrance window of 105 mm diameter (see Figs. 2 and 3). The total length of the HPD is 67 mm.

The sapphire window, which has excellent mechanical and optical properties (its refractive index is almost matched to the one of the scintillator crystal), is brazed to a metallic ring made of niobium, which assures the connection to the photocathode. A set of two electrodes in niobium (0.7 mm thick) inserted in between cylindrical alumina spacers (ceramic) promise a precise 1:1 electron optical image transfer from the photocathode onto the Si sensor.

At the base of the body, a skirt in kovar is welded to a stainless steel flange with a sharp knife designed to close the detector at the end of photocathode processing using a cold indium sealing technique. All the metallic components are joined with the ceramic rings in a single active high-temperature brazing step.

Fig. 3. Photograph of the sealed PET-HPD prototype tube. The Al-coated Si sensor is clearly visible.

The inner lateral surfaces of the ceramic rings receive a special surface treatment[6] to control their resistivity and avoid undesirable charging up effect.

On the base plate a ceramic hybrid carrier is mounted, which supports the sensor and the readout chips (VATAGP5, developed by IDEAS[7] in collaboration with CERN).

[5]A rectangular tube with improved active area fraction is foreseen at a later stage of the project.

[6]Photonis-DEP, Brive La Gaillarde, France.

[7]Ideas ASA, Fornebu, Norway.

The control and data connections for the encapsulated ASICs are realized by wire bonding to 40 vacuum feed troughs in the base plate.

Details of the evaporation plant facility at CERN and the photocathode processing can be found in Ref. [6].

2.2. The sensor

The sensor consists of a 300 μm thick rectangular plate of high-resistivity Si (~5 kΩ cm) produced by SINTEF[8] with 16×13 pads implemented as p^+n junctions, DC coupled to the front end electronic. The 208 pads of $3.98 \times 3.98\,mm^2$ with a gap of 20 μm match precisely the crystal matrix configuration. They are arranged in two halves of 8×13 pads for the readout, separated by 2 mm. The pad size is larger than the crystal bar cross section ($3.2 \times 3.2\,mm^2$) to cope with the light spread on the photocathode due to the finite thickness of the window.

The average load capacity of a pad, including the capacity of the neighbouring pads, routing lines and the capacity to the back plane, was measured to be about 5 pF for full depletion ($V_{bias} > 30$ V). The leakage current per pad is around 500 pA.

2.3. The VATA-GP5 chip

The front end electronics is an integral component of the PET concept consisting of two VATA-GP5 chips of 128 channels each, encapsulated in the HPD body as described above. The chip was designed to be operated in a self-triggering mode with a sparse readout option to optimize the data-taking rate in a high counting-rate environment (up to 2 MHz per HPD).

Each channel of the VATA-GP5 features a charge sensitive pre-amplifier/amplifier optimized for a detector capacitance of 5–7 pF and an input leakage current compensation, automatically and individually adjusted. The total dynamic range extends to 1.2 pC for positive input polarity. The analogue value of a hit channel and the associated channel address can be read out in four different modes: serial (by multiplexing all channels), sparse (by addressing only the hit channels), sparse with adjacent channels and sparse with reading any selection of channels.

The analogue chain is a classical arrangement where a Sample and Hold (S/H) signal is applied at the peaking time (adjustable between 200 and 250 ns) of the *slow* shaper when a trigger is detected, in order to store the analogue value for later readout.

In the *fast* chain, the signal from the fast shaper of ~40 ns peaking time is applied to a discriminator implemented with a *time walk compensation* circuit to minimize the time walk of the discriminator for different signal amplitudes. The outputs of the 128 discriminators are OR'ed together and provide the trigger (Fast OR (FOR)) for the data acquisition or the possibility of detecting coincidences with an expected timing resolution of less than 10 ns.

When a discriminator is activated, the analogue values of the hit channels with their address will be read out.

There is a common threshold for all the 128 discriminators, but a fine adjustment of each threshold is possible by means of a 3-bit DAC.

While the sparse readout is an essential feature to maximize the data acquisition rate, the serial readout is needed to test the correct functioning of all the channels, to register occasionally the pedestals for subtraction, and to measure the electronic and detector noise.

In the sparse mode, data acquisition speed is determined by the readout clock frequency, currently limited to 20 MHz.

2.4. The data acquisition system

Data acquisition is performed by a VME interface. A VME slave card, A24 and D32 type, has been built for this purpose. This card generates the three sequences of clocks necessary for the three types of read-out: serial, sparse and sparse with adjacent channels. It contains two pipelined 10 bit ADCs, the first for data in the serial and sparse mode, and the second for sparse with adjacent channels mode.

3. Results from test of the first proto-type PET-HPD

The performance of the VATA-GP5 chip has been characterized and the fully assembled proto-type PET–HPD has been evaluated in a specifically instrumented test set-up.

3.1. Results from measurements with VATA-GP5

Linearity of the amplifier/shaper chain and discriminator response were measured using the feature to inject sequentially into each channel a calibrated charge.

Fig. 4 displays the linearity of the VATA-GP5 amplifier/shaper response with the injected input charges. Above 1 pC, the observed saturation effect is due to the limited dynamic range of the ADC.

Fig. 5 shows the excellent linearity of the discriminator response. The plot has two *y*-axes. The left one corresponds to the measured charge in ADC counts. For the right axis, the calibration of the full electronic chain, which is discussed in Section 3.3, has been applied. A threshold of 20 mV—still a safe value avoiding any oscillations—allows detecting signals as low as 30 photoelectrons, corresponding to a 30 keV energy deposition in a LYSO crystal.

The data in Fig. 6, obtained with a threshold of 20 mV, prove that the time walk compensation circuit reduces the time dispersion of the discriminator to less than 10 ns for input charges above 30 fC. This limit corresponds to 50 detected pe's (or ~50 keV deposited energy) if the HPD is operated at 20 kV. Hence, the time walk performance matches the PET specific requirements.

[8]SINTEF, Forskningsveien 1, P124 Blindern, 0314, Norway.

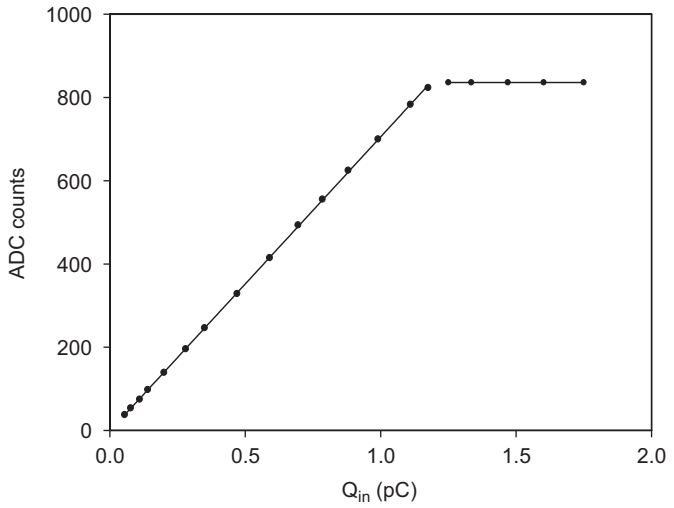

Fig. 4. Charge response (in ADC counts) vs. input charge Q_{in}.

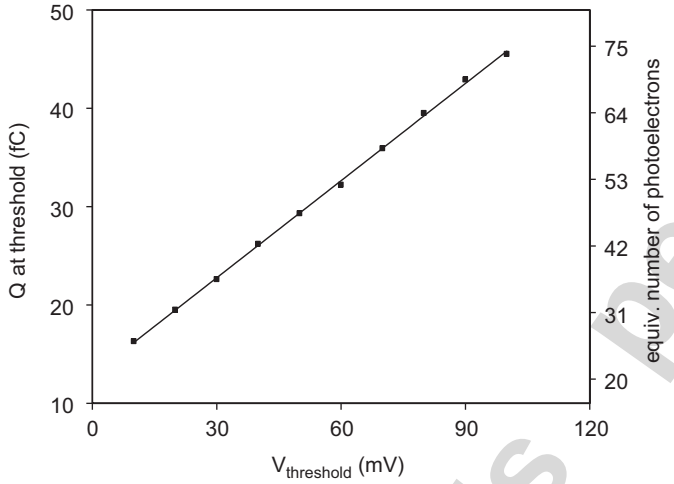

Fig. 5. Characteristics of the discriminator. Input charge i_{in} (ADC counts) versus threshold voltage U_{th} (mV). The preamplifier is operated with gain 'LO'. N_{pe} at threshold vs. U_{th}.

3.2. Experimental set-up

The prototype PET-HPD shown in Fig. 3 was tested using the set-up sketched in 7. Collimated (~5 mm ∅) blue light pulses (~470 nm peak wavelength) are generated by a LED (NICHIA-NSPB), which is fired at a 50 kHz rate. The pulse duration used for the tests was adjusted to 40 ns. This value is similar to the decay time of the LYSO crystals and, as will be shown below, leads to the number of detected photoelectrons (~500), which one would expect for a 511 keV γ converting in a LYSO crystal (Fig. 7).

The mirror, which reflects the light pulse onto the PET-HPD, could be rotated and translated to permit a scanning of the photocathode surface.

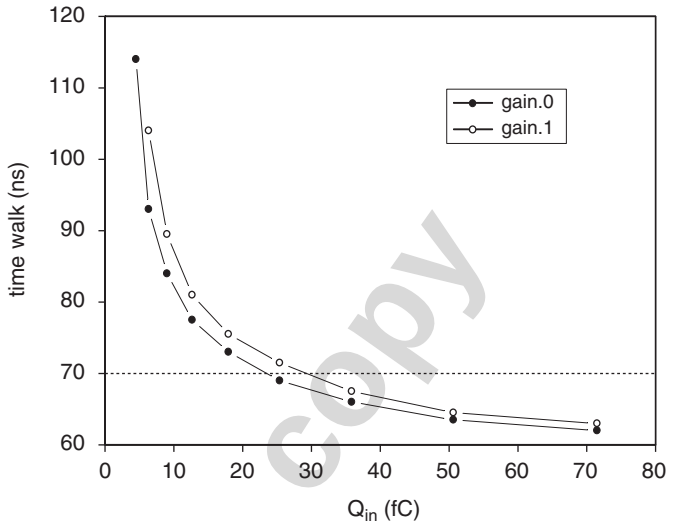

Fig. 6. Time walk (ns) vs. input charge (fC) for the two different gain stettings.

3.3. Experimental results

The set-up allows to scan the light spot over the cathode surface and to establish a mapping between the cathode and the Si sensor. This is shown in Fig. 8 for a scan in the y-direction. The results in x-direction are fully comparable. The mapping function is well described by a linear function. The observed deviations are of the order of 60 μm (RMS).

Fig. 9 shows a Lego plot of the hit distribution of the hit pads for cathode voltages of −10 and −20 kV. At −20 kV, the charge on some of the neighbor's pads exceeds the discriminator threshold and consequently increases the hit pad multiplicity; however, 90% of the light spot intensity is concentrated on two pads (chip 1, addresses 45 and 53). The threshold (~20 fC) eliminates any dark current of the photocathode, which would consist of single photoelectrons and leads to background-free images.

The total charges measured as the sum of the charges induced on all hit pads above the threshold at −10 and −20 kV are displayed in Fig. 10, including Gaussian fits.

The variation of the mean detected charge μ for the two main hit pads 45 and 53 is plotted in Fig. 11 as a function of the cathode voltage U_C. The Si bias voltage is set at 40 V, well above the value for full depletion. The relation is linear; however, it intercepts with the x-axis at $U_C = -6$ kV due to the relatively thick non-active layer (Al/n^+) at the sensor entrance, which can be improved in a future sensor production. The specific energy loss depends on the initial energy of the electrons,[9] i.e. on the cathode voltage. At 20 kV an energy loss $\Delta E = 1.6$ keV is expected. The

[9]See e.g. stopping power and energy loss tables provided by NIST http://physics.nist.gov.

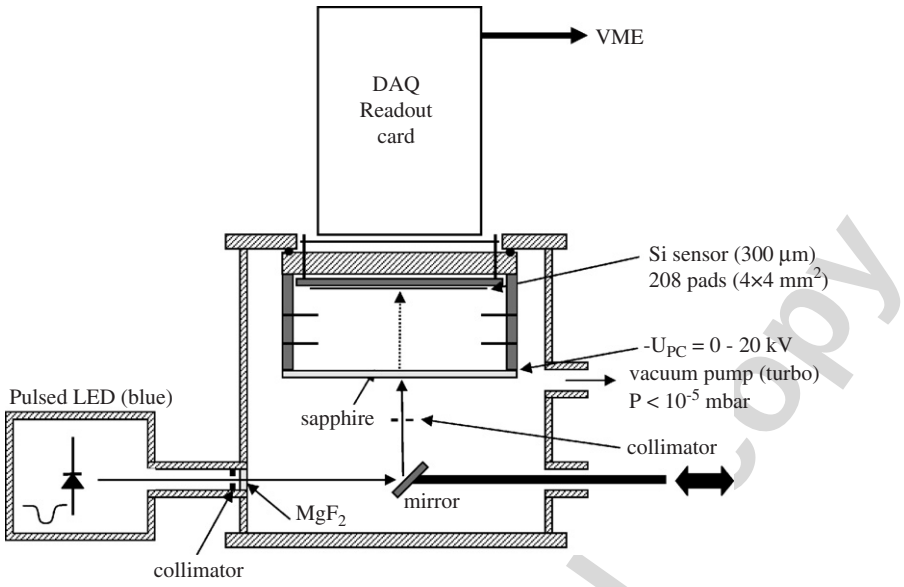

Fig. 7. Set-up to test the PET-HPD with a pulsed LED.

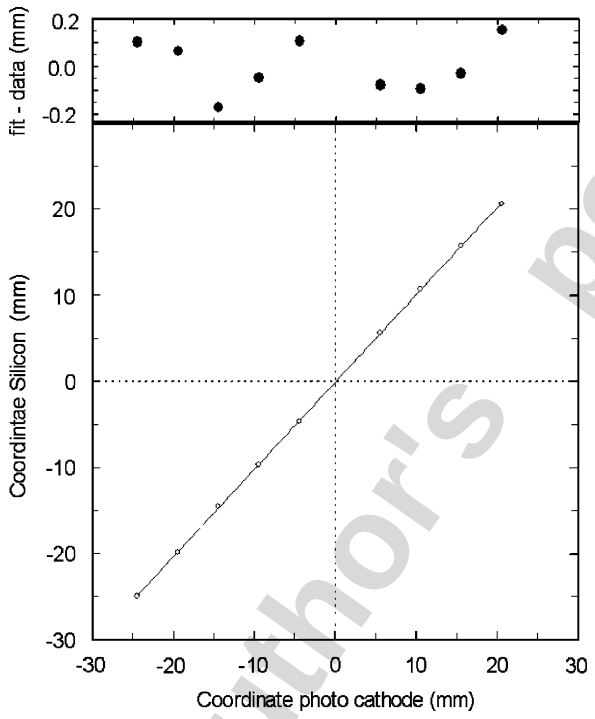

Fig. 8. Mapping between photocathode and Si sensor. The relation is purely linear, deviations are of the order of 60 μm (RMS).

intrinsic gain of the HPD $g = (E - \Delta E)/w$ at 20 kV is then 5090.

The ratios σ/μ vs. U_C, shown in the same plot for the same two pads, clearly exhibit the straggling effect due to the energy loss in the inactive entrance layer of the Si sensor (see discussion in Section 2). The asymptotic values of the ratio (for $U_C \to \infty$) yield the number of photoelectron according to $\sigma/\mu = (\mathrm{ENF}/N)^{1/2}$. We found 507 and 378 for the pads #45 and #53, respectively. From these values, and knowing the HPD gain at 20 kV ($g = 5090$), we calculated the absolute calibration of the electronic chain i.e. the equivalent charge per ADC count. For chip 1 we obtain 0.94 ± 0.01 fC/ADC count, the calibration of chip 2 is about 7.6% lower.

4. Conclusions

We designed, fabricated and tested a prototype HPD with a set of features and characteristics that are optimized for the readout of a scintillator matrix in a novel PET concept. The 1:1 electron–optical mapping between the photocathode and the Si sensor should allow for unambiguous identification of the hit scintillator crystal. The tube can be operated at 20 kV, providing a gain of about 5000. We demonstrated all relevant features of the custom-designed readout chip VATA-GP5. The complete electronic chain was energy calibrated in an absolute way. The system has an appropriate dynamic range that will allow detecting energy deposits from 30 to well above 511 keV in a LYSO crystal and shows very good linearity. Time walk is efficiently suppressed to better than ± 5 ns.

The fabrication of a second PET-HPD tube is under preparation. The next major step in the project is to assemble a complete camera module consisting of a crystal matrix and two HPDs in order to characterize its spatial and energy resolution.

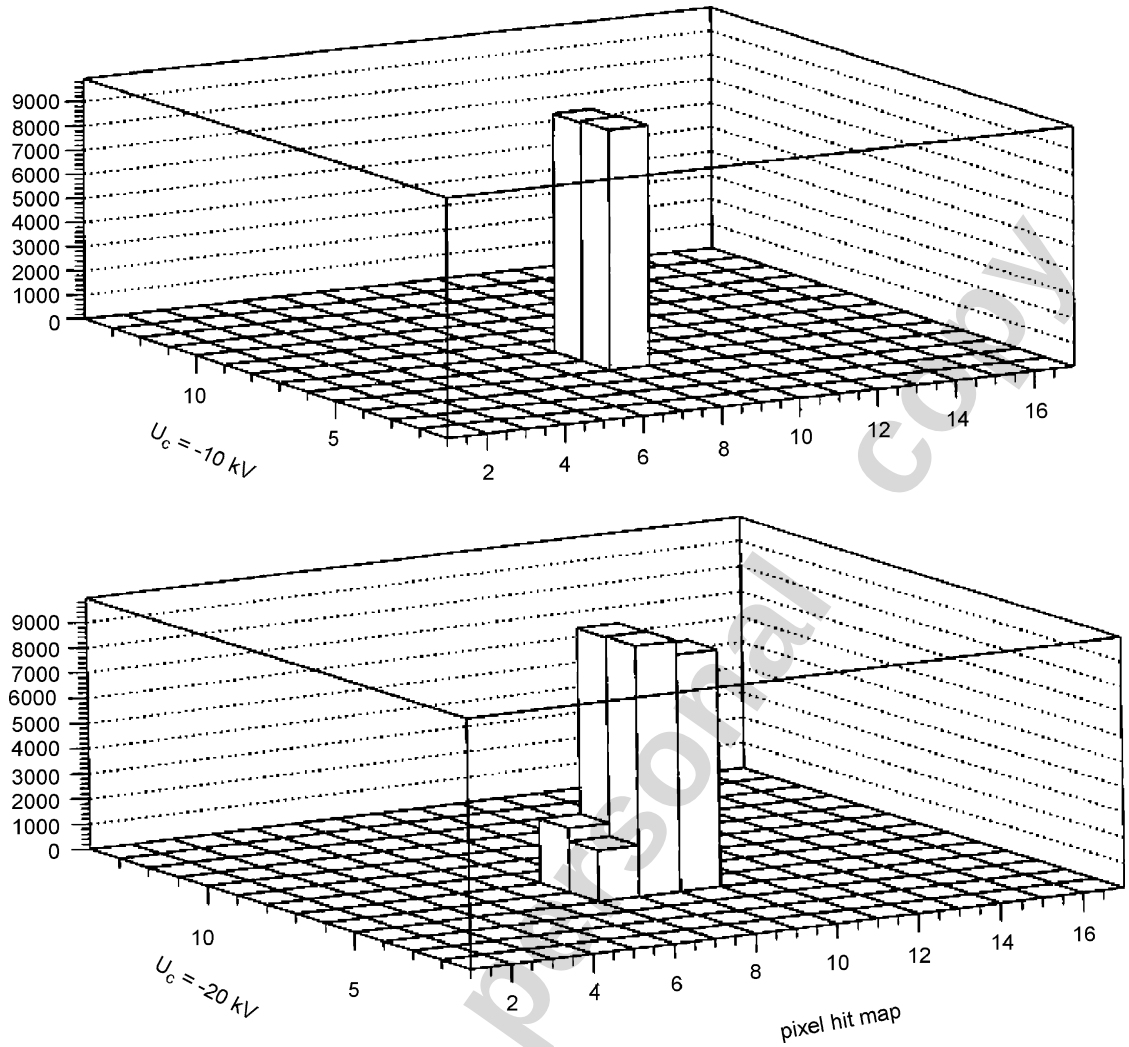

Fig. 9. PET-HPD hit maps at $U_C = -10$ and -20 kV.

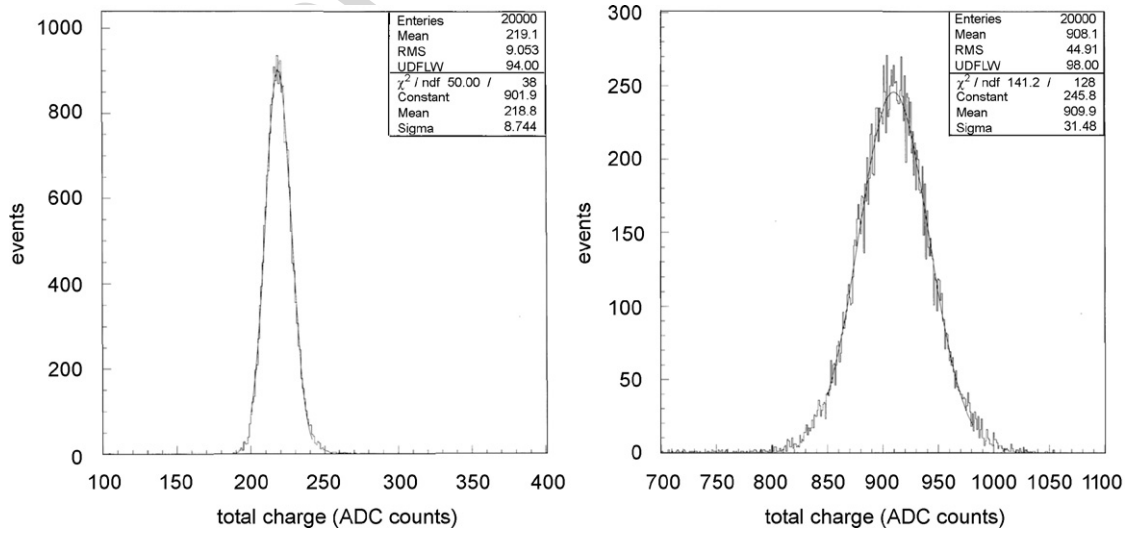

Fig. 10. Histograms of the total charge for two different HPD acceleration voltages. Left: $U_C = -10$ kV; Right: $U_C = -20$ kV.

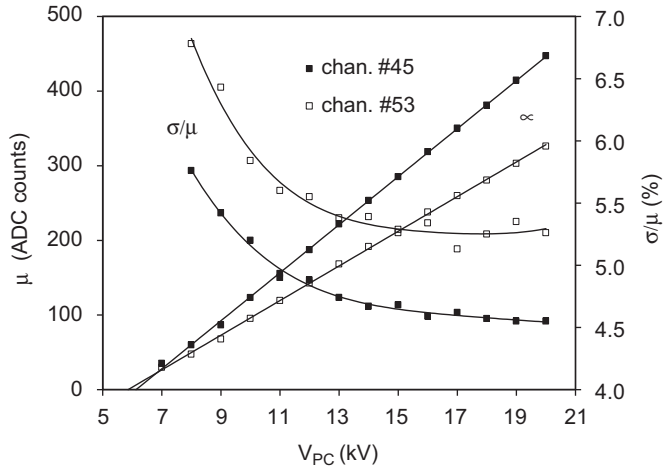

Fig. 11. Mean charge μ (left axis) and ratio of Gaussian width to mean charge σ/μ (right axis) versus cathode voltage U_C (kV).

Acknowledgements

We would like to thank our technical staff, F. Cossey, C. David, I. McGill and M. van Stenis, (all CERN) for their excellent work in the preparation of the mechanical, optical and electronic detector components.

References

[1] J. Seguinot, A. Braem, E. Chesi, C. Joram, S. Mathot, P. Weilhammer, M. Chamizo Llatas, J.G. Correia, M. Ribeiro da Silva, F. Garibaldi, R. De Leo, E. Nappi, F. Corsi, A. Dragone, F. Schoenahl, H. Zaidi, Novel geometrical concept of a high performance brain PET scanner—principle, design and performances estimates, IL Nuovo Cimento, Vol. 29C, N.4 Luglio-Agosto 2006.

[2] A. Braem, M. Chamizo Llatas, E. Chesi, J.G. Correia, F. Garibaldi, C. Joram, S. Mathot, E. Nappi, M. Ribeiro da Silva, F. Schoenahl, J. Seguinot, P. Weilhammer, H. Zaidi, Phys. Med. Biol. 49 (2004) 2547.

[3] M. Chamizo Llatas, A. Braem, E. Chesi, C. Joram, S. Mathot, J. Seguinot, P. Weilhammer, F. Garibaldi, E. Nappi, F. Schoenahl, H. Zaidi, High resolution 3D brain PET with hybrid photon detector, in: Proceedings of eight ICATTP Conference on Astroparticle, Particle, Space Physics, Detectors and Medical Imaging, World Scientific, Singapore, 2004, p. 391.

[4] I. Vilardi, A. Braem, E. Chesi, F. Ciocia, N. Colonna, F. Corsi, F. Cusanno, R. De Leo, A. Dragone, F. Garibaldi, C. Joram, L. Lagamba, S. Marrone, E. Nappi, J. Seguinot, G. Tagliente, A. Valentini, P. Weilhammer, H. Zaidi, Optimization of the effective light attenuation length of YAP:Ce and LYSO:Ce crystals for a novel geometrical PET concept, Nucl. Instr. and Meth. A 564 (2006) 506.

[5] A. Braem, E. Chesi, C. Joram, J. Seguinot, P. Weilhammer, Development of HPDs for Applications in Physics and medical imaging, Nucl. Instr.and Meth. A 567 (2006) 162.

[6] A. Braem, C. Joram, F. Piuz, E. Schyns, J. Seguinot, Nucl. Instr. and Meth. A 502 (2003) 205.